

Influences of quenching treatment and cobalt-doping on the thermally activated flux-flow behavior in $\text{KCa}_2(\text{Fe}_{1-x}\text{Co}_x)_4\text{As}_4\text{F}_2$

Yixin Liu^{1,2}, Teng Wang^{1,3}, Zulei Xu^{1,2}, Wenshan Hong^{4,5}, Wei Peng^{1,2} , Zhi-Rong Lin^{1,2}, Huiqian Luo^{4,*}  and Gang Mu^{1,2,*} 

¹ State Key Laboratory of Functional Materials for Informatics, Shanghai Institute of Microsystem and Information Technology, Chinese Academy of Sciences, Shanghai 200050, People's Republic of China

² University of Chinese Academy of Sciences, Beijing 100049, People's Republic of China

³ School of Physical Science and Technology, ShanghaiTech University, Shanghai 201210, People's Republic of China

⁴ Beijing National Laboratory for Condensed Matter Physics, Institute of Physics, Chinese Academy of Sciences, Beijing 100190, People's Republic of China

⁵ International Center for Quantum Materials, School of Physics, Peking University, Beijing 100871, People's Republic of China

E-mail: hq Luo@iphy.ac.cn and mugang@mail.sim.ac.cn

Received 22 March 2023, revised 4 July 2023

Accepted for publication 11 July 2023

Published 21 July 2023



Abstract

Owing to the unique double-FeAs-layered structure between neighboring insulating layers, the 12442-type Fe-based superconductors are expected to host rich vortex phenomena in the mixed state. Here, we report a systematic investigation on the influences of quenching treatment and cobalt-doping on the magnetic vortex dynamics of $\text{KCa}_2(\text{Fe}_{1-x}\text{Co}_x)_4\text{As}_4\text{F}_2$ ($x = 0, 0.1$) single crystals via electrical transport measurements. It is found that the slopes of the upper critical field near T_c , $d\mu_0 H/dT|_{T_c}$ along both directions ($H \perp c$ and $H \parallel c$), are doubled by the cobalt-doping with $x = 0.1$. The activation energy is acquired by analyzing the Arrhenius plots, which shows a $H^{-\alpha}$ dependence with a change in the exponent α at around 3 T, indicating the evolution of the dominant pinning mechanisms in different field regions. Importantly, the quenching treatment obviously enhances the magnitude of activation energy and critical current density J_c , which can be suppressed by the introduction of cobalt-doping. Possible mechanisms for such evolutions of these important parameters are discussed. Our results emphasize the important role of quenching treatment in enhancing the activation energy and critical current density in 12442 system.

Supplementary material for this article is available [online](#)

Keywords: Fe-based superconductors, TAFF behavior, quenching treatment, critical current density

(Some figures may appear in colour only in the online journal)

* Authors to whom any correspondence should be addressed.

1. Introduction

Fe-based superconductors (FeSCs) [1–4] are regarded as the second family of high-temperature superconductors, which share similar features to the cuprate superconductors. It is known that the crystal structure can have fundamental influences on the electronic structure and physical performance of the unconventional superconducting (SC) systems [5]. With the SC critical temperature T_c of 28–37 K, the 12442-type $AB_2Fe_4As_4C_2$ ($A = K, Rb, \text{ and } Cs$; $B = Ca, Nd, Sm, Gd, Tb, \text{ and } Ho$; and $C = F \text{ and } O$) compounds [6–9] reveal the unique double-FeAs-layered structure. The physical properties of this system have been investigated intensively in recent years [10–21]. Among them, an important aspect is about the vortex dynamics. In our previous studies, a very steep slope of the upper critical field near T_c and a strong Pauli-paramagnetic effect in $KCa_2Fe_4As_4F_2$ have been reported [10, 11]. The second magnetization peak were revealed both in the $RbCa_2Fe_4As_4F_2$ and $KCa_2Fe_4As_4F_2$ systems by the magnetization measurements [22–24]. Recent scanning tunneling microscopy measurements have revealed the Friedel oscillations of vortex bound states and a new type of vortex pattern with bamboo-like chains in confined canals in the $KCa_2Fe_4As_4F_2$ compound [25, 26]. In addition, we have observed a significant suppression of the activation energy for the flux flow in the ultra-thin sample of $KCa_2Fe_4As_4F_2$ [12]. The correlation between the activation energy and the SC anisotropy in FeSCs was also uncovered [27].

Between the upper critical field and irreversible field in the H – T phase diagram, vortices are in the liquid state [28]. In this region, a thermally activated flux-flow (TAFF) behavior was frequently observed [22, 29–33], in terms of a linear relation between $\ln\rho$ and $1/T$. Here ρ is the resistivity of the superconductor in the vortex-liquid state. Thus the activation energies U_0 could be extracted from Arrhenius plots ($\ln\rho$ vs. $1/T$). In addition, by investigating the evolution of U_0 with magnetic field, important information concerning the dimensionality of the vortex state and the type of the pinning centers could be obtained [22]. Typically the nature of vortex pinning in layered superconductors is susceptible to the inner defects, which can be affected by chemical doping and/or growing process. Currently there is still a lack of investigations concerning the influences of these factors on the vortex behaviors of 12442-type superconductors.

In this paper, we conducted the electrical transport measurements on high-quality $KCa_2(Fe_{1-x}Co_x)_4As_4F_2$ ($x = 0, 0.1$) single crystals grown under different conditions. It is found that the slope of the upper critical field H_{c2} near T_c and the anisotropy of H_{c2} are both enhanced by the doping of cobalt. The activation energies shows a $H^{-\alpha}$ dependence. The exponent α reveals different values in the low and high field regions, indicating that the change of defect types that play a dominant role in pinning the vortices. Moreover, the quenching treatment and the introduction of cobalt-doping are found to have obvious influences on the magnitude of activation energy and critical current density.

2. Experimental details

High quality $KCa_2(Fe_{1-x}Co_x)_4As_4F_2$ ($x = 0, 0.1$) single crystals were grown using KAs as the self-flux. The detailed synthesis conditions and the characterizations of the samples can be seen in our previous reports [10, 18]. Notably, two different procedures were adopted in the cooling process. For the non-quenched samples, after the high-temperature solid-state reaction, the stainless steel tube containing reactants was cooled down slowly to room temperature. While for the quenched ones, the samples were removed from furnace to be cooled down rapidly to room temperature after a slowly cooling process from 980 °C to 900 °C. The introduction of cobalt dopant was achieved by partially replacing the reagent Fe_2As with Co_2As . The doping levels used in this work are the nominal values.

The structures of the obtained samples were evaluated using a DX-2700 type x-ray diffractometer. The electrical resistance was measured using a four-probe technique on a physical property measurement system (Quantum Design). The electrical current was applied within the ab -plane of the samples. The direction of the current is always perpendicular to that of the magnetic field. The applied current density is about $4 \mu A \mu m^{-2}$ during the resistivity measurements. The magnetization measurements were carried out on the magnetic property measurement system (Quantum Design, MPMS 3). In the present study, we measured a series of samples obtained under different growth conditions. In order to provide a clear impression, we summarized the information of these samples in table 1.

3. Results

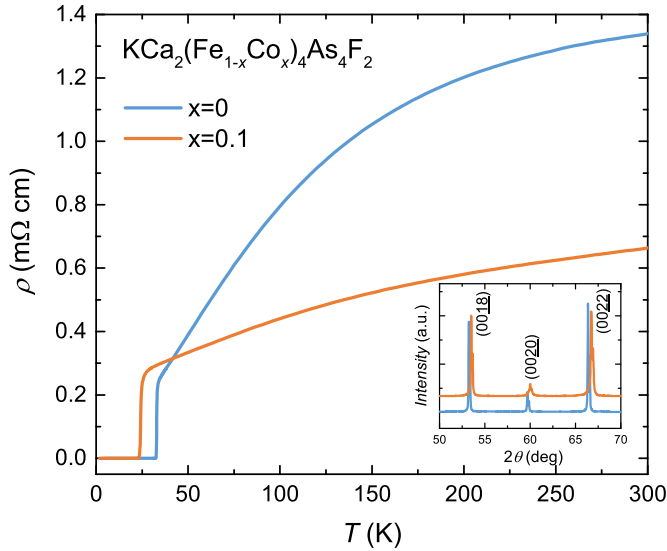
3.1. Characterization

The x-ray diffraction patterns are shown in the inset of figure 1. Only sharp peaks along (00 $2l$) direction can be seen, indicating a high c -axis orientation of the crystals. Notably, the introduction of Co-dopant did not cause the appearance of impurities or precipitates. Moreover, the diffraction peaks of the sample with $x = 0.1$ are shifted to higher angles as compared with the undoped one, suggesting the shrinkage of crystal lattice along the c -axis. A quantitative analysis shows that the c -axis lattice constant is reduced by about 0.44%. This tendency is consistent with that reported in the polycrystalline samples of Co-doped $KCa_2Fe_4As_4F_2$ [34], which is also very similar to that reported in the Co-doped $CaFeAsF$ system [35].

Temperature dependence of resistivity for two samples with $x = 0$ and 0.1 is shown in figure 1. It is found that the quenching treatment has no significant influence on the SC transition of the samples. Thus, only the data of the quenched samples are shown here. By the introduction of Co-doping with $x = 0.1$, the SC transition temperature T_c is suppressed from 33.8 ± 0.5 K to 24.4 ± 0.4 K. Here the values of T_c are determined using the criteria of $90\% \rho_n$, where ρ_n is the normal-state

Table 1. Summary of the information of the samples measured in the present study.

Name	x	Growth mode	$n(H_{c2})$	$n(U_0)$	$n(J_c)$
UnD-Non-n	0	Non-quenched	—	1	2
UnD-Qu-n	0	Quenched	0	1, 2	3
CoD-Qu-n	0.1	Quenched	0	1, 2, 3	4

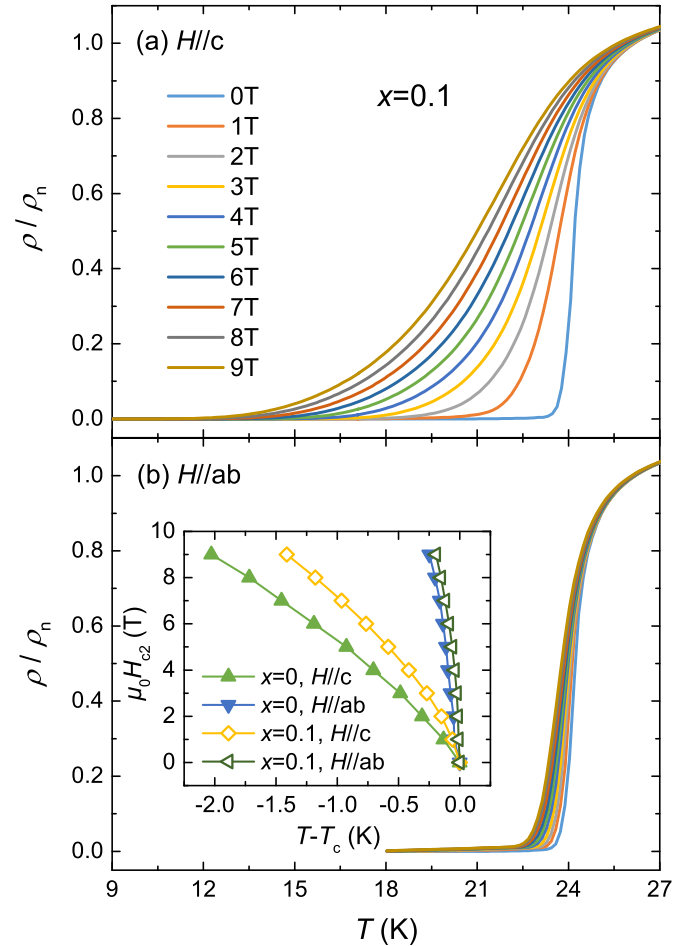
**Figure 1.** Temperature dependence of resistivity of the $\text{KCa}_2(\text{Fe}_{1-x}\text{Co}_x)_4\text{As}_4\text{F}_2$ ($x = 0, 0.1$) single crystals under zero magnetic field. Both samples are quenched ones. The inset shows the XRD patterns of the two samples.

resistivity near the SC transition. The deviation of T_c values comes from small fluctuations between different samples. Such a decrease of T_c induced by Co-doping is consistent with the results based on the polycrystalline samples [34]. It is a common feature of unconventional superconductors that T_c is closely dependent on carrier concentration. We noted that the undoped $\text{KCa}_2\text{Fe}_4\text{As}_4\text{F}_2$ is self-hole-doped with a doping level of 0.25. Thus the introduction of Co-doping with $x = 0.1$ pushes the total hole content to 0.15. The accompanying decrease of T_c implies that co-doping pushes the system away from the optimal doping position, although the exact point of optimal doping is still unknown.

Another distinct feature is the different evolution tendencies of the resistivity with temperature in the normal state between the two samples, which results in an intersection point at around 41 K. Meanwhile, the residual resistivity ratio, $\text{RRR} = \rho_{300\text{K}}/\rho_n$, is reduced from 5.5 to 2.4 by the Co-doping with $x = 0.1$. We note that this tendency is also consistent with that observed in the polycrystalline samples [34].

3.2. Upper critical field

To study the influence of co-doping on the upper critical field, we performed the measurements on temperature dependence of electrical transport with the magnetic field along two different orientations: $H \parallel c$ and $H \parallel ab$. As the upper critical

**Figure 2.** (a), (b) Normalized resistivity for the sample with $x = 0.1$ as a function of temperature under the magnetic field up to 9 T with $H \parallel c$ and $H \parallel ab$, respectively. The inset of (b) shows the comparison of the upper critical fields H_{c2} as a function of $T - T_c$ between two samples with $x = 0$ and 0.1.

field of the undoped sample has been studied in our previous work [10], here we only display the resistivity data of the sample with $x = 0.1$. As shown in figures 2(a) and (b), the SC transition point shifts to lower temperature with the increase of the magnetic field for both orientations. In addition, such a shift is much more quickly when the magnetic field is applied along the c axis, revealing a significant anisotropic characteristic.

Using the criteria of $90\% \rho_n$, the values of upper critical H_{c2} are extracted. In order to have an intuitive comparison with the undoped sample, the obtained H_{c2} is drawn as a function of $T - T_c$, as shown in figure 2(c). It can be seen that, in both orientations, the data of the sample with $x = 0.1$ always reveals a steeper increasing tendency in the vicinity of T_c ,

Table 2. Summary of the detailed parameters about T_c and upper critical fields for the two samples with different doping levels.

Sample	T_c (K)	$\mu_0 H'_{c2, ab}$ (T K ⁻¹)	$\mu_0 H'_{c2, c}$ (T K ⁻¹)	Γ	G_i ($\times 10^{-2}$)
UnD-Qu-0 ^a	33.3	-50.9	-6.4	8.0	2.8
CoD-Qu-0	25.0	-122.8	-13.3	9.2	3.3

^a The data of this sample are cited from our previous work [10].

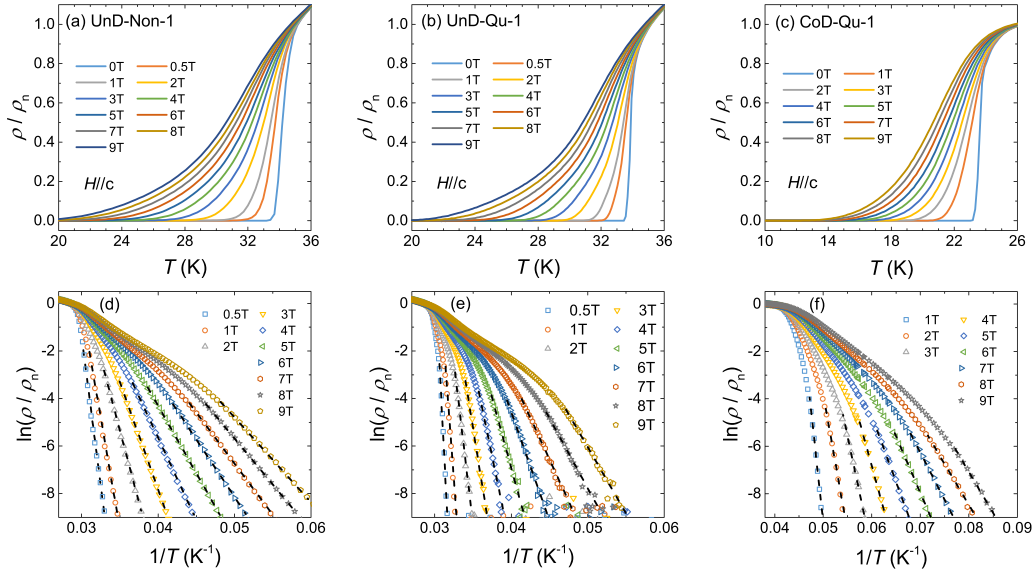


Figure 3. Normalized resistivity (a)–(c) and the corresponding Arrhenius plots (d)–(f) for three samples (UnD-Non-1, UnD-Qu-1, and CoD-Qu-1) under the magnetic field parallel to the c -axis. The black dashed lines are the fits with TAFF theory to the experimental data.

i.e. $T - T_c = 0$. Quantitatively, the slope of the tangent in the H_{c2} - T curves near T_c , $\mu_0 H'_{c2} \equiv d\mu_0 H_{c2}/dT|_{T_c}$, is -122.8 and -13.3 T K⁻¹ for the orientations of $H \parallel ab$ and $H \parallel c$ respectively. We note that these values are about two times of that reported in the undoped sample [10]. In addition, the anisotropy Γ of the upper critical field near T_c can be estimated from these two values, which is 9.2 for the sample with $x = 0.1$. It is slightly larger than that of the undoped sample, indicating that the introduction of Co-doping enhances the anisotropy of the this system. Such a behavior is consistent with the result of electronic structure calculations which reveals the disappearance of a small three-dimensional Fermi pockets induced by co-doping (see figures 3(d)–(f) in [34]). These quantitative results are summarized in table 2.

The influence of thermal fluctuation on the magnetic vortex is quantified by the Ginzburg number, which can be expressed as [28, 37] (in the International System of Units) $G_i = (k_B/4\pi\mu_0)^2 (T_c/H_{c2}^2 \varepsilon \xi^3)^2 / 2 = 1.07 \times 10^{-13} \kappa^4 T_c^2 / \mu_0 H_{c2,||c} \varepsilon^2$. Here $H_c = H_{c2,||c} / \sqrt{2} \kappa$ is the thermodynamic critical field, $\kappa = \lambda / \xi$ is the Ginzburg–Landau parameter, λ is the in-plane London penetration depth, ξ is the in-plane SC coherence length, and $\varepsilon = 1/\Gamma$ is the anisotropy parameter. From values of $\mu_0 H'_{c2}$, the zero-temperature in-plane coherence length ξ can be estimated to be 1.5 and 1.2 nm for the samples with $x = 0$ and 0.1 respectively. Assuming a similar value of λ (~ 230 nm) [14] for the two samples, values of G_i is

calculated to be 2.8×10^{-2} and 3.3×10^{-2} for the two quenched samples with $x = 0$ and 0.1 respectively. These values are much larger than conventional superconductors and comparable to other systems of the FeSCs [36, 38], indicating a relatively remarkable fluctuation effect on the magnetic vortex in the present system.

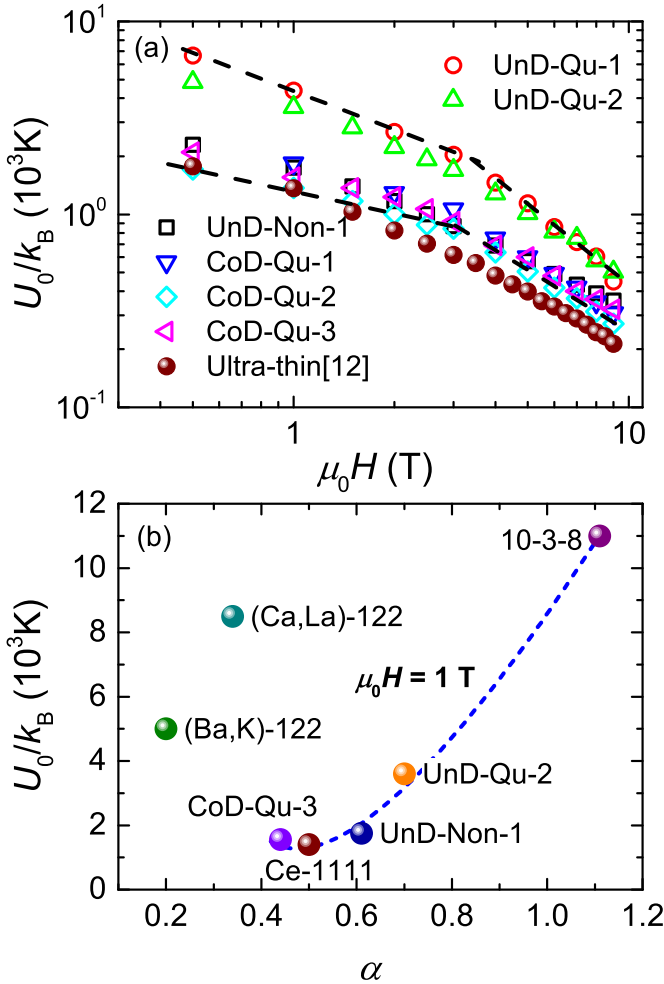
3.3. TAFF behavior

In order to investigate the influences of quenching treatment and co-doping on the TAFF behavior, we measured the resistivity of six samples under the vertical magnetic field. Temperature dependence of normalized resistivity for three samples (UnD-Non-1, UnD-Qu-1, and CoD-Qu-1) is shown in figures 3(a)–(c). The data of other samples are used to check the reproducibility of the experimental results, which can be seen in figure S1 in the supplementary material. The details of the six samples for the investigation of the TAFF behavior are summarized in table 1. We note here that sample CoD-Qu-1 reveals a slightly different T_c from that of sample CoD-Qu-0 as shown in figure 2. With the increase of field, the SC transition width is broadened significantly, revealing the active movements of the flux flow.

Figures 3(d)–(f) show the Arrhenius plots of the normalized resistivity for the three samples under different fields. As shown by the black dashed lines, $\ln(\rho/\rho_n)$ reveals a linear

Table 3. The value of power exponent α in $U_0 \propto H^{-\alpha}$ for the samples grown under different conditions.

Sample	α_l	α_h	$\alpha_h - \alpha_l$
UnD-Non-1	0.61	0.82	0.21
UnD-Qu-1,2	0.67–0.7	1.09–1.25	0.39–0.58
CoD-Qu-1,2,3	0.41–0.50	0.96–1.11	0.52–0.61


Figure 4. (a) Field dependence of U_0/k_B for six samples plotted in a double logarithm coordinate. The data of the ultra-thin sample [12] is also shown for a comparison. The black dashed lines represent the linear fits to the data of samples UnD-Qu-1 and CoD-Qu-2. (b) Values of U_0 at 1 T as a function of power exponent α . The data of other systems of FeSCs [36] are also displayed for a comparison. The blue dashed line is a guide for eyes.

dependence upon $1/T$ in a wide temperature region in all the three samples. The Arrhenius plots of other samples are shown in supplementary figure S2. This linear behavior is consistent with the theoretical prediction that the dissipations under magnetic field is induced by TAFF [29]. Such a TAFF behavior has been reported in other systems, including FeSCs [22], cuprates [29–32], and transition metal disulphides [33]. In the TAFF region where the linear behavior in $\ln(\rho/\rho_n) - 1/T$ is maintained, the values of activation energy U_0 can be extracted from the slopes of the Arrhenius plots.

The obtained values of U_0 are summarized in figure 4(a) in a double-logarithmic scale. Comparing the performances among these different samples, we can draw the following conclusions: (1) By comparing samples UnD-Non-1 with UnD-Qu-1 and UnD-Qu-2, it is clear that quenching treatment can significantly enhance the value of activation energy. (2) Co-doping leads to the decrease of activation energy, which can be seen from the comparison between the samples CoD-Qu-1, CoD-Qu-2, CoD-Qu-3 and UnD-Qu-1, UnD-Qu-2. In addition, as we have reported [12], the activation energy of ultra-thin samples is also significantly lower than that of bulk materials. For the bulk samples, U_0 follows a power law with the magnetic field with a clear change in the power exponent at around 3 T, i.e. $U_0 \propto H^{-\alpha_l}$ for $\mu_0 H < 3$ T, and $U_0 \propto H^{-\alpha_h}$ for $\mu_0 H > 3$ T. The black dashed lines in figure 4(a) represent such a evolutionary trend of samples UnD-Qu-1 and CoD-Qu-2 as the examples. The values of the power exponents α_l and α_h are summarized in table 3. Although there are some fluctuations in the data, we can still extract some important information from it. The α_l value of the co-doped samples is obviously smaller than that of the undoped ones. Moreover, the non-quenched sample shows the lowest value of α_h , resulting in a very small difference between α_h and α_l , i.e. $\alpha_h - \alpha_l = 0.21$.

3.4. Critical current density

The in-plane critical current density J_c for three samples was obtained by measuring the irreversible magnetization with $H \parallel c$. The values of J_c can be evaluated using the extended Bean model [39]

$$J_c = \frac{20(M_{\text{down}} - M_{\text{up}})}{a(1 - a/3b)}, \quad (1)$$

where M_{up} (emu cm^{-3}) and M_{down} (emu cm^{-3}) are the magnetization when sweeping the field up and down, respectively. a (cm) and b (cm) are the sample width and length, respectively. In figures 5(a) and (b), we show the isothermal hysteresis loop and the derived field dependence of J_c of sample UnD-Qu-3. No fishtails were observed, which suggests that the pinning is not weak in the present system. The self-field J_c at 2 K for sample UnD-Qu-3 is 6.3 MA cm^{-2} . The J_c values of non-quenched (UnD-Non-2) and Co-doped (CoD-Qu-4) samples are 1.4 and 0.9 MA cm^{-2} respectively (see figure 5(c)), being several times smaller than that of UnD-Qu-3. Such a behavior is consistent with the evolution tendency of U_0 among the three types of samples as shown in figure 4. We note that the J_c value of the sample UnD-Qu-3 is consistent with our previous report [13] and clearly larger than other systems in FeSCs, e.g. $\text{RbCa}_2\text{Fe}_4\text{As}_4\text{F}_2$ ($\sim 0.8 \text{ MA cm}^{-2}$) [22], $(\text{Ba,K})\text{Fe}_2\text{As}_2$ ($\sim 2.4 \text{ MA cm}^{-2}$) [40], $\text{CaKFe}_4\text{As}_4$ ($\sim 1.6 \text{ MA cm}^{-2}$) [41], and $(\text{Ca}_{0.85}\text{La}_{0.15})_{10}(\text{Pt}_3\text{As}_8)(\text{Fe}_2\text{As}_2)_5$ ($\sim 2.3 \text{ MA cm}^{-2}$) [36]. This indicates that the quenched sample has an important application prospect in high current transmission.

The field dependent evolution tendency of J_c can supply important information about the pinning mechanism. As shown by the black dashed lines in figure 5(c), in the field region above 0.7 T, J_c follows a power-law behavior with H ,

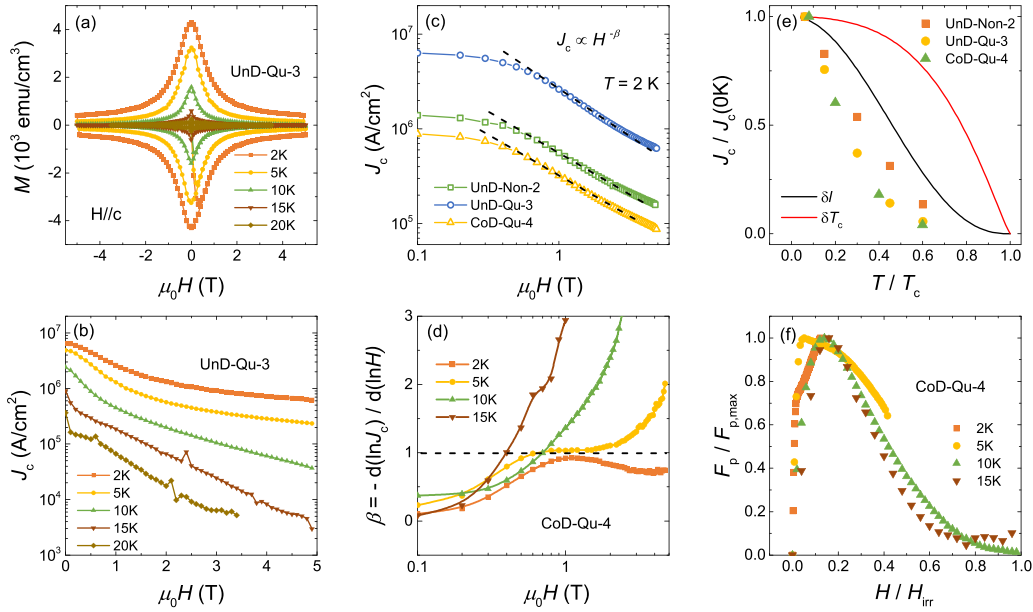


Figure 5. (a) Field dependence of magnetization for sample UnD-Qu-3 at various temperatures. The applied field is parallel to c axis. (b) Field dependence of in-plane J_c evaluated using the data shown in (a). (c) The data of J_c at a fixed temperature of 2 K in log-log scales for three samples. The black dashed lines show the power-law behaviors. (d) Field dependence of parameter β for sample CoD-Qu-4. (e) Temperature dependence of normalized self-field J_c of the three samples. The data are compared with the theoretical models based on the δl and δT_c pinning. (f) Normalized pinning force density ($F_p/F_{p,max}$) as a function of reduced field for sample CoD-Qu-4.

i.e. $J_c \propto H^{-\beta}$. The power parameters β in this field region for the three samples are 0.88, 0.99, and 0.90, respectively. Actually the field dependence of the J_c does not follow a pure power law in the whole field region. In order to display the detailed evolution of the parameter β with field, we plot the value $\beta = -d(\ln J_c)/d(\ln H)$ vs $\mu_0 H$ for the sample CoD-Qu-4 in figure 5(d). It can be seen that, in the low field region, β is below 0.5. With the increase of magnetic field, it shows a gradual upward trend. For the case of low temperature (2 and 5 K), the β - $\mu_0 H$ curves reveal a platform-like feature between 0.7–2 T. The very small value of β in the low field region was interpreted in terms of strong correlated pinning [42]. At the moderate field around 0.3 T, the value of β is about 0.5, which reflects the pinning from nm-sized defects. While at higher fields, only a fraction of the vortices can be pinned when the vortex density exceeds the density of the pinning centers. Moreover, the vortex displacements due to pinning become comparable to the vortex spacing and the critical current density starts to decrease more rapidly [42]. These two factors give rise to a relatively large value of β in the high field region.

As shown in figure 5(e), normalized critical current density ($J_c/J_c(0\text{ K})$) of the three samples is compared with the theoretical models based on the δl and δT_c pinning. Although the experimental data deviate from the predictions of both theoretical models, relatively speaking, the δl model can better reflect the trend of experimental fact. The pinning force density is determined by the value of J_c and the applied magnetic field H , $F_p = J_c \times \mu_0 H$. The field dependence of F_p normalized by its maximum value $F_{p,max}$ of sample CoD-Qu-4 is shown in figure 5(f). It can be seen that, at low temperatures (2 and 5 K), the $F_p/F_{p,max}$ - H/H_{irr} curves show the sign of multi-peak structure, which may be related to the self-field

effects [43]. The positions of the peaks are all at the low values of $H/H_{irr} (< 0.2)$, which is lower than that reported in $\text{Ba}(\text{Fe},\text{Co})_2\text{As}_2$ system [38]. Actually, considering the relation $J_c \propto H^{-\beta}$, the field dependence of pinning force density can be expressed as $F_p \propto H^{1-\beta}$. Consequently, F_p will increase with H in the field region where $\beta < 1$, while it can be expected to decrease with H when $\beta > 1$. In this sense, the systematic evolution of the $F_p/F_{p,max}$ with H/H_{irr} actually reflects the variation of the exponent β with field, and the positions of the peaks in this figure correspond to the situations where $\beta = 1$. The rather low values of H/H_{irr} for the peak positions may indicate that, although the pinning effect at each pinning center is strong, the density of the pinning center is relatively small, resulting in the decrease of F_p at a rather small magnitude of magnetic field.

4. Discussion

It is known that the power-law dependence of U_0 on the field is a characteristic for the 3D flux liquids [12, 22, 30, 32]. Based on this picture, the values of power exponents α_l and α_h are closely related with the type of defects that dominate the flux pinning behaviors and/or the pinning modes of the vortices [22, 30]. From the general understanding, the magnitude of α_l in the low field region of about 0.5 could be interpreted by the domination of strong pinning by the planar defects. On the other hand, the magnitude of α_h is around 1 when the magnetic field is above 3 T, which is an index for the domination of the weak pinning by the point defects. Actually, the presence of planar defects has been confirmed by the scanning transmission electron microscopy analysis in the quenched

samples [13]. It is notable that the value of α_h for sample UnD-Non-1 is clearly smaller than 1, indicating the deviation from the pure pinning mode based on point defects.

It is also important to compare our data with the behavior of other systems of FeSCs. In figure 4(b), we show values of activation energy U_0 as a function of power exponent α under a low field of 1 T. The values of α_l are used here for the three samples in 12442 system. The data of other systems in FeSCs [36], including (Ba,K)Fe₂As₂, (Ca,La)Fe₂As₂, CeFeAs(O,F), and (Ca_{0.85}La_{0.15})₁₀(Pt₃As₈)(Fe₂As₂)₅, are also displayed for a comparison. These systems are referred to as (Ba,K)-122, (Ca,La)-122, Ce-1111, and 10-3-8, respectively. It can be seen that, for the 10-3-8, Ce-1111, and 12442 (UnD-Qu-2, UnD-Non-1, and CoD-Qu-3) systems, the evolution of U_0 with α follows a roughly positive correlation trend. The two samples of 122 system, which have a much smaller anisotropy, obviously deviated from this trend. This shows that anisotropy is an important factor affecting the TAFF behavior of layered superconductors.

Another noteworthy issue is that the introduction of cobalt doping has not brought about an increase in the activation energy. On the contrary, the activation energy is reduced. This indicates that, although the cobalt doping leads to a suppression of RRR , the additional defects from the substitutions have not significantly enhanced the pinning force to the vortices. One possible explanation for this behavior is that the spatial scale of defects caused by Co-doping is too small to act as an effective pinning center for the vortices. Typically the defects induced by impurities or ion irradiations should have a size of several to tens of nanometers to supply the effective pinning centers [13, 44]. Another factor worthy of attention is that the activation energy shows an anti-correlation with the anisotropy in the FeSCs [27]. Thus, the enhancement of Γ from 8.0 to 9.2 induced by Co-doping may be the dominant and intrinsic reason for the reduction of U_0 in Co-doped samples.

5. Conclusion

In summary, we have studied the upper critical field, TAFF behavior, and critical current density of KCa₂(Fe_{1-x}Co_x)₄As₄F₂ ($x = 0, 0.1$) single crystals grown under different conditions. The activation energy U_0 was extracted from the Arrhenius plots. It is found that the value of U_0 is obviously enhanced by the quenching process of the crystal growth. Meanwhile, the introduction of Co-doping leads to the reduction of U_0 . The power exponent α changes its value at around 3 T, revealing the evolution of the dominant types of defects in pinning the vortices. Moreover, the critical current density J_c of the non-quenched sample with $x = 0$ is several times smaller than that of the quenched one, which indicates a relatively weaker flux pinning in the non-quenched samples and further confirms the conclusion drawn from data of activation energy. Our results reveal the significant effect of quenching process on enhancing the activation energy and critical current density of 12442 system, which is of valuable for the practical applications.

Data availability statement

All data that support the findings of this study are included within the article (and any supplementary files).

Acknowledgments

This work is supported by the Youth Innovation Promotion Association of the Chinese Academy of Sciences (Grant Nos. 2015187 and Y202001), the National Key Research and Development Program of China (Grant No. 2018YFA0704200), and the Strategic Priority Research Program (B) of the CAS (Grant No. XDB25000000). The experimental measurements were supported by the Superconducting Electronics Facility (SELF) of Shanghai Institute of Microsystem and Information Technology.

ORCID iDs

Wei Peng  <https://orcid.org/0000-0002-9888-1891>

Huiqian Luo  <https://orcid.org/0000-0003-1514-0041>

Gang Mu  <https://orcid.org/0000-0001-5676-4702>

References

- [1] Kamihara Y, Watanabe T, Hirano M and Hosono H 2008 *J. Am. Chem. Soc.* **130** 3296
- [2] Rotter M, Tegel M and Johrendt D 2008 *Phys. Rev. Lett.* **101** 107006
- [3] Hsu F-C et al 2008 *Proc. Natl Acad. Sci.* **105** 14262
- [4] Zhu X, Han F, Mu G, Cheng P, Shen B, Zeng B and Wen H-H 2009 *Phys. Rev. B* **79** 220512(R)
- [5] Mizuguchi Y, Hara Y, Deguchi K, Tsuda S, Yamaguchi T, Takeda K, Kotegawa H, Tou H and Takano Y 2010 *Supercond. Sci. Technol.* **23** 054013
- [6] Wang Z-C, He C-Y, Wu S-Q, Tang Z-T, Liu Y, Ablimit A, Feng C-M and Cao G-H 2016 *J. Am. Chem. Soc.* **138** 7856
- [7] Wang Z-C, He C-Y, Wu S-Q, Tang Z-T, Liu Y, Ablimit A, Tao Q, Feng C-M, Xu Z-A and Cao G-H 2017 *J. Phys.: Condens. Matter* **29** 11LT01
- [8] Wang Z-C, He C-Y, Tang Z-T, Wu S-Q and Cao G-H 2017 *Sci. China Mater.* **60** 83
- [9] Wang Z-C, He C-Y, Wu S-Q, Tang Z-T, Liu Y and Cao G-H 2017 *Chem. Mater.* **29** 1805
- [10] Wang T et al 2019 *J. Phys. Chem. C* **123** 13925
- [11] Wang T et al 2020 *Sci. China Phys. Mech. Astron.* **63** 227412
- [12] Zhang C et al 2021 *2D Mater.* **8** 025024
- [13] Pyon S, Kobayashi Y, Takahashi A, Li W, Wang T, Mu G, Ichinose A, Kambara T, Yoshida A and Tamegai T 2020 *Phys. Rev. Mater.* **4** 104801
- [14] Yu A B, Wang T, Wu Y F, Huang Z, Xiao H, Mu G and Hu T 2019 *Phys. Rev. B* **100** 144505
- [15] Terashima T et al 2020 *Phys. Rev. B* **102** 054511
- [16] Hong W et al 2020 *Phys. Rev. Lett.* **125** 117002
- [17] Wu D et al 2020 *Phys. Rev. B* **101** 224508
- [18] Chu J, Wang T, Zhang H, Liu Y, Feng J, Li Z, Jiang D, Mu G, Di Z and Xie X 2020 *Chin. Phys. Lett.* **37** 127401
- [19] Duan W, Chen K, Hong W, Chen X, Yang H, Li S, Luo H and Wen H-H 2021 *Phys. Rev. B* **103** 214518
- [20] Zhang C et al 2022 *Sci. China Phys. Mech. Astron.* **65** 237411
- [21] Hao J, Hong W, Zhou X, Xiang Y, Dai Y, Yang H, Li S, Luo H and Wen H-H 2022 *Phys. Rev. B* **106** 014523

- [22] Xing X, Yi X, Li M, Meng Y, Mu G, Ge J-Y and Shi Z 2020 *Supercond. Sci. Technol.* **33** 114005
- [23] Lopes P V, Sundar S, Salem-Sugui Jr. S, Hong W, Luo H and Ghivelder L 2022 *Sci. Rep.* **12** 20359
- [24] Yi X, Xing X, Meng Y, Zhou N, Wang C, Sun Y and Shi Z 2023 *Chin. Phys. Lett.* **40** 027401
- [25] Chen X, Duan W, Fan X, Hong W, Chen K, Yang H, Li S, Luo H and Wen H-H 2021 *Phys. Rev. Lett.* **126** 257002
- [26] Duan W, Chen K, Hong W, Chen X, Li S, Luo H, Yang H and Wen H-H 2022 *Nano Lett.* **22** 9450
- [27] Yu A B et al 2021 *Chin. Phys. B* **30** 027401
- [28] Blatter G, Feigel'man M V, Geshkenbein V B, Larkin A I and Vinokur V M 1994 *Rev. Mod. Phys.* **66** 1125
- [29] Vinokur V M, Feigel'man M V, Geshkenbein V B and Larkin A I 1990 *Phys. Rev. Lett.* **65** 259
- [30] Zou X, Wang Z, Chen J and Zhang H 2001 *Physica C* **356** 31
- [31] Brunner O, Antognazza L, Triscone J-M, Miéville L and Fischer Ø 1991 *Phys. Rev. Lett.* **67** 1354
- [32] Qiu X G, Wuyts B, Maenhoudt M, Moshchalkov V V and Bruynseraede Y 1995 *Phys. Rev. B* **52** 559
- [33] Zhang H, Fang Y, Wang T, Liu Y, Chu J, Li Z, Jiang D, Mu G, Di Z and Huang F 2021 *Phys. Rev. B* **103** L180503
- [34] Ishida J, Iimura S and Hosono H 2017 *Phys. Rev. B* **96** 174522
- [35] Ma Y H, Hu K K, Ji Q C, Gao B, Zhang H, Mu G, Huang F Q and Xie X M 2016 *J. Cryst. Growth* **451** 161
- [36] Choi W, Seo Y, Ahmad D and Kwon Y S 2020 *Results Phys.* **19** 103430
- [37] Iida K, Hänisch J and Tarantini C 2018 *Appl. Phys. Rev.* **5** 031304
- [38] Putti M et al 2010 *Supercond. Sci. Technol.* **23** 034003
- [39] Gyorgy E M, van Dover R B, Jackson K A, Schneemeyer L F and Waszczak J V 1989 *Appl. Phys. Lett.* **55** 283
- [40] Taen T, Ohtake F, Pyon S, Tamegai T and Kitamura H 2015 *Supercond. Sci. Technol.* **28** 085003
- [41] Pyon S et al 2019 *Phys. Rev. B* **99** 104506
- [42] van der Beek C J, Konczykowski M, Abal'oshev A, Abal'osheva I, Gierlowski P, Lewandowski S J, Indenbom M V and Barbanera S 2002 *Phys. Rev. B* **66** 024523
- [43] Lehtonen J, Mikkonen R and Perälä R 2004 *Physica C* **401** 151
- [44] Sarkar A, Dang V, Mikheenko P, Kechik M A, Abell J and Crisan A 2010 *Thin Solid Films* **519** 876